New Phytologist

Research

Rare pits, large vessels and extreme vulnerability to cavitation in a ring-porous tree species

Mairgareth A. Christman[1], John S. Sperry[2] and Duncan D. Smith[2]

[1]Institute for Ecohydrology Research, 1111 Kennedy Place Ste 4, Davis, CA 95616, USA; [2]Department of Biology, University of Utah, 257 South 1400 East, Salt Lake City, UT 84112, USA

Author for correspondence:
John S. Sperry
Tel: +1 801 585 0379
Email: j.sperry@utah.edu

Received: *9 September 2011*
Accepted: *19 October 2011*

New Phytologist (2012) **193**: 713–720
doi: 10.1111/j.1469-8137.2011.03984.x

Key words: air-seeding mechanism, drought responses, ecological wood anatomy, embolism refilling, rare pit hypothesis, ring-porous trees, vulnerability curves, xylem cavitation.

Summary

- The rare pit hypothesis predicts that the extensive inter-vessel pitting in large early-wood vessels of ring-porous trees should render many of these vessels extremely vulnerable to cavitation by air-seeding. This prediction was tested in *Quercus gambelii*.
- Cavitation was assessed from native hydraulic conductivity at field sap tension and in dehydrated branches. Single-vessel air injections gave air-seeding pressures through vessel files; these data were used to estimate air-seeding pressures for inter-vessel walls and pits.
- Extensive cavitation occurred at xylem sap tensions below 1 MPa. Refilling occurred below 0.5 MPa and was inhibited by phloem girdling. Remaining vessels cavitated over a wide range to above 4 MPa. Similarly, 40% of injected vessel files air-seeded below 1.0 MPa, whereas the remainder seeded over a wide range exceeding 5 MPa. Inter-vessel walls averaged 1.02 MPa air-seeding pressure, similar and opposite to the mean cavitation tension of 1.22 MPa. Consistent with the rare pit hypothesis, only 7% of inter-vessel pits were estimated to air-seed by 1.22 MPa.
- The results confirm the rare pit prediction that a significant fraction of large vessels in *Q. gambelii* experience high probability of failure by air-seeding.

Introduction

Plant water transport relies on the movement of water through dead xylem conduits. The conductivity of the water transport system is related to the diameter of vessels raised to the fourth power according to the Hagen–Poiseuille relationship. As such, the larger the vessels, the greater the potential conductivity of the plant xylem network. However, large vessels also have disadvantages. In addition to potential mechanical tradeoffs (wider vessels can be more susceptible to implosion by sap under tension and may weaken wood), large vessel diameters increase the risk of cavitation by freezing stress (Sperry & Tyree, 1988; Tyree & Sperry, 1989; Cochard & Tyree, 1990).

Ring-porous xylem exemplifies the tradeoff between vulnerability and conductivity. In ring-porous species, a band of very wide early-wood vessels is produced early in the growing season, followed by much narrower late-wood vessels. Early-wood vessels of ring-porous trees are quite vulnerable to winter embolism and generally function for just one growing season (Zimmermann, 1983). Only as a new layer of early-wood is produced in the late spring will bud break occur, and the delay in the growing season is consistent with the protection of the new early-wood vessels from spring freezes (Zimmermann & Brown, 1971; Wang *et al.*, 1992).

There is also considerable evidence that larger vessels are more vulnerable to cavitation by water stress, although the relationship can be quite variable (Tyree *et al.*, 1994; Pockman & Sperry, 2000; Hacke *et al.*, 2006). An important cause of cavitation by water stress is the spread of air from embolized conduits through inter-conduit pits (the 'air-seeding' mechanism). A current model explains vessel vulnerability as a combination of the quality and quantity of the inter-conduit pits. In terms of quality, thicker and less porous pit membranes are associated with greater resistance to cavitation by air-seeding because more pressure is required to pull air across them (Lens *et al.*, 2010). In terms of quantity, the more pits per vessel, the more vulnerable the vessel. This latter relationship is explained by the 'rare pit' hypothesis, which presumes that not all of the thousands of inter-conduit pits in a vessel are exactly alike. The safety of a vessel depends on the single leakiest pit and, by probability, that rare pit will be leakier when there are more pits in the vessel. In support of the rare pit hypothesis, there is a significant relationship between pit area per vessel and increasing vulnerability across species. Residual variation is, in theory, attributable to differences in pit quality across species (Hargrave *et al.*, 1994; Choat *et al.*, 2003; Wheeler *et al.*, 2005; Hacke *et al.*, 2006).

According to the rare pit hypothesis, a significant number of the large early-wood vessels in a ring-porous tree are likely to be very vulnerable to cavitation. These large vessels would necessarily have a very large number of inter-vessel pits, increasing the probability of extremely leaky pits in at least some of them. Indeed, typical techniques of studying vulnerability to cavitation,

such as centrifugation and pressure-sleeve air injection, generally indicate that ring-porous species cavitate significantly at modest sap tensions (< 1.0 MPa; Bush *et al.*, 2008; Li *et al.*, 2008). Accordingly, ring-porous trees at midday would be operating with several of their current year's early-wood vessels cavitated. Nevertheless, their midday stem conductivity can be roughly comparable with co-existing diffuse-porous species, and at least some species may be able to refill their cavitated vessels overnight (Taneda & Sperry, 2008).

However, the presence of highly vulnerable vessels in ring-porous or other large-vesseled taxa has been questioned because of potential problems with the centrifuge and pressure-sleeve methods (Cochard *et al.*, 2005, 2010; Choat *et al.*, 2010; Ennajeh *et al.*, 2011). These methods induce cavitation in the middle portion of excised stem segments. Long vessels could conduct microbubbles or other nucleators into the center of the segment, triggering cavitation in the centrifuge or outgassing with the pressure sleeve. Premature cavitation in these long vessels could cause the so-called '*r*'-shaped rise in the loss of conductivity at the beginning of vulnerability curves, making the xylem appear more vulnerable than it is *in vivo*.

In this paper, we report a thorough investigation of the vulnerability of early-wood xylem vessels in stems of the ring-porous Gambel oak (*Quercus gambelii*) using methods that should be immune to an open-vessel artifact. This species was chosen because our earlier work has shown it has an '*r*'-shaped centrifuge vulnerability curve and operates at high levels of native embolism (Bush *et al.*, 2008; Li *et al.*, 2008; Taneda & Sperry, 2008). We looked for diurnal changes in native conductivity associated with cavitation and refilling, and determined the effect of phloem girdling on the process. We compiled a dehydration vulnerability curve, the 'gold standard' of methods (Cochard *et al.*, 2010). In the dehydration protocol, xylem sap tensions are induced naturally by the transpiring plant *in vivo*, and in detached branches allowed to dry. In addition, we probed the vulnerability of individual vessel endwalls to air-seeding using the single-vessel technique (Zwieniecki *et al.*, 2001), and employed the results to estimate the vulnerability of vessel endwalls and inter-vessel pits to air-seeding using a simple probability model (Christman *et al.*, 2009). If cavitation occurs by air-seeding, the dehydration curve should be linked to the air-seeding behavior of individual vessels.

Materials and Methods

Plant material

Approximately 5–8-yr-old saplings (3–4 m tall) of *Quercus gambelii* Nutt. were studied from the Red Butte Canyon near the University of Utah in Salt Lake City, UT, USA (40°46′23″N, 111°49′12″W, 1565 m). Observations were made from 22 June to mid-August 2009. The study population consisted of a single stand extending *c.* 0.5 km along a road and exposed to sun at midday. Most of the measurements required the sacrifice of saplings, and the availability of suitable material limited the sample size of some experiments.

Stem hydraulic conductivity measurements

Stem hydraulic conductivity was obtained by measuring the flow rate of 20 mM KCl solution in filtered (0.2 μm) purified water (not degassed) through excised, unbranched stem segments at a known hydraulic pressure gradient. Unless noted, all conductivity segments were 27.5-cm-long portions of the trunk or main branches of the saplings and were 3–5 yr old and *c.* 10–15 mm in diameter. Segments were attached to a tubing system and passive uptake (water absorption by the sample) at a zero pressure gradient was measured gravimetrically. A pressure head of < 2 kPa was induced to drive flow through the segment while not displacing air from any vessels continuous through the stem segments. After the pressure-induced flow had been measured, the rate of passive uptake was re-measured. The process was repeated until the 'before' and 'after' passive uptake rates were similar, at which point they were averaged and subtracted from the pressurized flow rate to obtain the net pressure-driven flow rate. The net pressure-driven flow rate was divided by the pressure gradient to obtain the hydraulic conductivity. Slightly negative conductivities can result when cavitation is extensive and pressurized flow is negligible compared with the average passive uptake. Conductivity was further standardized by the cross-sectional area of the stem (stem area-specific conductivity). We do not report the percentage loss of conductivity (PLC) relative to the maximum after embolism reversal (Sperry *et al.*, 1988) because the older growth rings of the segment were embolized by previous winters, and their refilling creates an artificially high maximum conductivity reference. There is no evidence that these older vessels refill naturally, and they are eventually occluded by tyloses (usually after 2 yr in *Q. gambelii* at the study site).

Native conductivity and dehydration vulnerability curve

A dehydration curve was compiled from measurements of the native conductivity at native sap tensions and conductivity in detached saplings that were dried to sap tensions above the maximum measured in the field (*c.* 1.5 MPa). To measure native conductivity, the base of the sapling was cut underwater by sealing a split funnel around the stem, filling with distilled water and cutting the stem under water with clippers. The cut sapling was rapidly transferred (< 1 s) into a tray of water where the other end was cut underwater. The excised stem segments were kept underwater in plastic bags during immediate transport to the laboratory. In the laboratory, the conductivity segment was cut from the harvested stem underwater and measured. Measurements were made at predawn and midday on eight dates over the summer (from 26 June to 4 August) to cover the physiological range of native stem sap tension.

The stem xylem tension corresponding to the native conductivity was measured before the sapling was excised. Three leaves or short shoots were sampled per tree. Leaves were covered with aluminum foil for at least 20 min before collection to stop transpiration and promote equilibration of leaf with stem xylem sap tension. Foil was used rather than plastic to avoid overheating of the covered leaves. Leaves were sampled below the conductivity

segments to avoid the possibility of creating emboli in stems when leaves were cut for tension measurements. Sap tensions were measured in a pressure chamber (PMS Instruments, Albany, OR, USA). Throughout this paper, we refer to sap tensions (a positive number) rather than the negative sap pressure to simplify comparison with the positive air-seeding pressures measured with the single-vessel method (see the section 'Single-vessel air injections').

To obtain sap tensions above the native range, saplings were covered in humidified plastic bags and cut at the base in air before rapidly being transported to the laboratory. Before bagging and cutting, three leaves or short shoots per branch were covered tightly in aluminum foil for subsequent measurement of sap tension. In the laboratory, branches were dried to a range of tensions. At this point, the sap tension was measured on the three bagged leaves, and the conductivity segment was cut from the branch underwater. The segment was located at a sufficient distance from the cut end of the sapling (> 1 m) to prevent the creation of additional emboli when the sapling was cut. Branches were collected between 22 and 25 June.

The mean cavitation tension and median tension (P50) were calculated from a best-fit Weibull function to the vulnerability data. We used bootstrapping to propagate uncertainty in the curve fit to the mean and median tensions. The original conductivity vs tension dataset was sampled randomly with replacement to generate bootstrapped datasets with the same number of data points as the original. Mean and median cavitation tensions were calculated for 1000 bootstrapped datasets and 95% confidence intervals were estimated as the 2.5 and 97.5 percentiles.

Vessel refilling and phloem girdling experiments

The presence of refilling was determined by comparing native area-specific conductivities at midday with predawn values. To test for the effect of phloem girdling, in the late afternoon (15:00–17:00 h, 9 July), 10 conductivity segments were identified on saplings in the field. Five were randomly chosen for a girdling procedure in which a circumferential 2-cm band of bark was carefully shaved away with a razor blade. Girdles were made above and below the conductivity segment. The exposed tissue was covered with a layer of silicone grease and wrapped in parafilm to prevent desiccation. The following morning at predawn all 10 stem segments were cut from the trees under water and their hydraulic conductivities were measured.

Two all-night vigils were held to determine whether positive sap pressures could be detected in some or all of the early-wood vessels. Periodically during the night, stems were cut and the attached end was quickly observed with a hand lens for sap exudation. Logistics (safety concerns) required that these nocturnal observations be made 3 km up the watershed from the main study population.

We attempted to induce refilling after it had ceased later in the season (after 4 August) by manipulating stem sap tensions in the field. Thin reflective sheets ('space blankets') were draped over several saplings beginning at mid-afternoon, and the sap tension and stem conductivity were measured after several hours of shading to assess the extent of hydration and refilling. In a separate experiment, we attempted to hydrate a clump of saplings overnight. Clusters of *Q. gambelii* stems are generally connected underground via lignotubers. To hydrate the cluster, we cut one of the stems underwater and supplied water to the rooted stump overnight. The degrees of hydration and refilling were assessed the next morning at predawn on the remaining saplings in the cluster.

Single-vessel air injections

Stems were cut underwater to a length of 75 cm and flushed from the youngest end with 20 mM KCl solution for 40 min at *c.* 75 kPa to hydrate the stem. A microcapillary tube was pulled to create tips approximating the diameter of early-wood xylem vessels (80–200 μm), and inserted into a vessel from the youngest end of the stem. This young end was of the same size and age range as the standard conductivity segment. The microcapillary was secured using superglue (Loctite 409 and 412). The other end of the capillary was connected to polyetheretherketone (PEEK) tubing connected to a pressure chamber, which allowed precise control of the slow increase in air pressure in the microcapillary. Before beginning measurements, air at 50 kPa was applied to check whether the vessel was open at both ends. If no air bubbles were observed at the other end of the stem under water, air was slowly raised at a rate of *c.* 100 kPa/7–8 s until air penetrated the stem. After the bubble pressure was reached, the superglue and capillary were carefully removed so that another vessel could be injected. Only large early-wood vessels in the current year's growth ring were tested, and each stem was only tested for air-seeding pressures on the day it was collected from the field. As many vessels as could be measured per day were tested (50–88 vessels per stem, eight stems overall, measurements during June–August 2009).

Early-wood vessel lengths

A vessel length distribution was created using 1.52-m-long stem segments of the approximate age and diameter as those employed for single-vessel air-seeding experiments. Five stems were cut in the field and flushed with 20 mM KCl solution at *c.* 70 kPa for *c.* 45 min. Flushed stems were injected overnight from the youngest end with a 10 : 1 mix of silicone : hardener mixed with optical brightener, as described in Hacke *et al.* (2006). Stem cross-sections were taken at five locations between 0.01 and 1.5 m from the injected end, with the percentage of early-wood vessels filled with silicone determined for each section. The vessel length distribution for the early-wood was determined from the rate at which the silicone-filled early-wood vessels declined with distance from the injected end using the method described in Christman *et al.* (2009).

Prediction of inter-vessel wall and pit air-seeding distributions from single-vessel air injection data

The stem air-seeding probability model developed in Christman *et al.* (2009) was modified to predict the distribution of endwall

and pit air-seeding pressures from the single-vessel injections. An injection gave the air-seeding pressure through a 75-cm-long file of early-wood vessels with at least one inter-vessel wall. A cumulative distribution function (CDF) for these file air-seeding pressures was determined from the best-fit Weibull function to the empirical data. This 'file-failure CDF_f' is a function of the endwall failure CDF_e and the number of inter-vessel walls ('endwalls' for short) per file (e) that must be breached. Assuming that the endwall failure pressure is independently distributed across all early-wood vessel files, the CDF_f evaluated at any air-seeding pressure p will be:

$$CDF_f(p) = \sum_{e=1}^{e\max} [CDF_e(p)^e n_e] \qquad \text{Eqn 1}$$

($e$max,maximum number of endwalls in any early-wood vessel file for the 75-cm stem length tested; $CDF_e(p)$, cumulative frequency of endwalls seeding at air pressure p; n_e, fraction of early-wood files in the stem of $e > 1$ with e endwalls present). The variables e, $e$max and n_e were obtained from the vessel length distribution discretized into nine logarithmically scaled length classes to represent the always short-skewed vessel distribution (Zimmermann, 1983). Vessels of a file were assumed to have uniform length (= the mid-length of the class), and files composed of uniform vessels were assumed to be staggered with respect to each other so that their endwall position was evenly distributed axially along the stem. Accordingly, the integer value of the quotient of stem length over vessel length yielded the minimum number of endwalls per file, and the remainder of the quotient yielded the fraction of those vessels with an additional endwall. For example, files of 36.6-cm vessels in a 75-cm-long stem would have a minimum of $e = 2$ endwalls (75/36.6 = 2.05), with 5% of those files having $e = 3$ endwalls. Because of discretization of the vessel length into classes, e increased in jumps across classes (Table 1). An Excel (Microsoft) macro was written by the second author to solve for $CDF_e(p)$ from Eqn 1, where $CDF_f(p)$ was represented by the best-fit Weibull distribution to the air injection data.

The endwall failure CDF_e, in turn, can be expressed as a function of the individual pit failure CDF_p, assuming that the pit failure pressure is independently distributed within and across all endwalls of all early-wood vessels:

$$CDF_e(p) = \sum_{i=1}^{i=\max} [1 - (1 - CDF_p(p))^{u_i}] n_i \qquad \text{Eqn 2}$$

($CDF_e(p)$, cumulative frequency of endwalls failing at air pressure p; i = max, number of vessel length and endwall classes (nine length classes split into e and $e + 1$ fractions); $CDF_p(p)$, cumulative frequency of all inter-vessel pits failing at air pressure p; u_i, number of endwall pits for the vessel length class; n_i, fraction of all of the endwalls in the stem that belong to vessel length and endwall class i). n_i was obtained from the vessel length distribution and e estimation. To estimate u_i (Table 1), we solved for the number of pits per vessel in each of the nine vessel length classes that resulted in the previously estimated average inter-vessel pit area in early-wood vessels (0.224 mm^2 from Hacke *et al.*, 2006; see Christman *et al.*, 2009 for details). We assumed that each individual pit had an area of 17.2 μm^2, based on microscopic observations. Equation 2 was solved for $CDF_p(p)$ based on estimates for all the other variables (Table 1).

Table 1 Vessel statistics used to estimate the air-seeding distribution of inter-vessel walls (= endwalls) and pits from single-vessel injections in *Quercus gambelii* (Eqns 1, 2)

Length class	Length (m)	Frequency	Pits per endwall (u_i)	Endwalls per file (e, n_e)
1	0.0019	0.009061	7	e = 389,390 n_e = 0.013,< 0.001
2	0.0055	0.017078	21	e = 136,137 n_e = 0.020,0.005
3	0.0157	0.032445	61	e = 47,48 n_e = 0.015,0.033
4	0.0449	0.061664	173	e = 16,17 n_e = 0.027,0.063
5	0.1283	0.11479	496	e = 5,6 n_e = 0.026,0.142
6	0.3664	0.196225	1415	e = 2,3 n_e = 0.272,0.013
7	1.0464	0.268006	4041	e = 1 n_e = 0.372
8	2.9884	0.224669	11542	
9	8.53494	0.076061	32965	

Bootstrapping was used to estimate confidence intervals for the mean and median pressures derived from the modeled CDF_e and CDF_p distributions. The air injection dataset was sampled with replacement to generate 1000 bootstrapped Weibull CDF_f curve fits, each yielding a corresponding CDF_e and CDF_p with a mean and median pressure. The 95% confidence intervals around the mean and median were estimated as the 2.5 and 97.5 percentiles from the 1000 bootstrapped estimates.

Statistics

Means were compared with 't' tests, with a significance threshold of $P = 0.05$. Sample sizes were constrained by the destructive nature of the experiments and limited sapling numbers. Means are cited ± SE when they were determined directly from measurements. Means or medians derived from curve fits and Eqns 1, 2 are cited with 95% confidence intervals (lower, upper) determined from bootstrapping.

Results

Native conductivities, vessel refilling and girdling effects

Native stem conductivity (per cross-sectional area) was extremely variable, but showed a decline from predawn (xylem tensions typically < 0.5 MPa; Fig. 1, open circles) to midday (tensions to

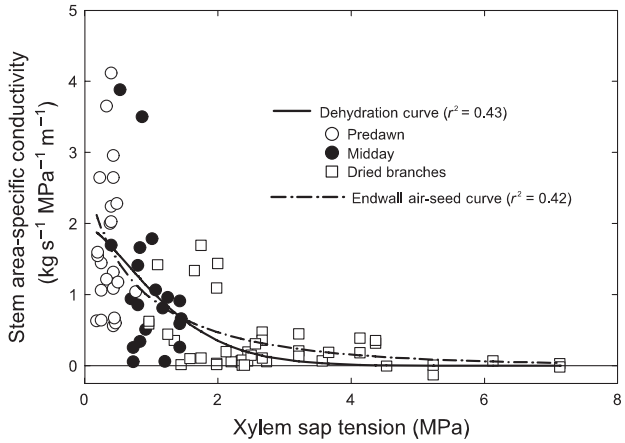

Fig. 1 Dehydration vulnerability to embolism curve for *Quercus gambelii* stems showing hydraulic conductivity per cross-sectional stem area as a function of xylem sap tension (= negative sap pressure). Symbols and solid curve (Weibull function) represent the dehydration vulnerability curve; each data point is a separate stem segment collected at predawn, midday or from excised drying branches. The dash–dotted line is the best fit of the endwall air-seeding distribution (Fig. 5, CDF_e) to the dehydration data (conductivity = k·[1 − CDF_e], where k is the curve-fitting parameter representing the maximum native conductivity). CDF, cumulative distribution function.

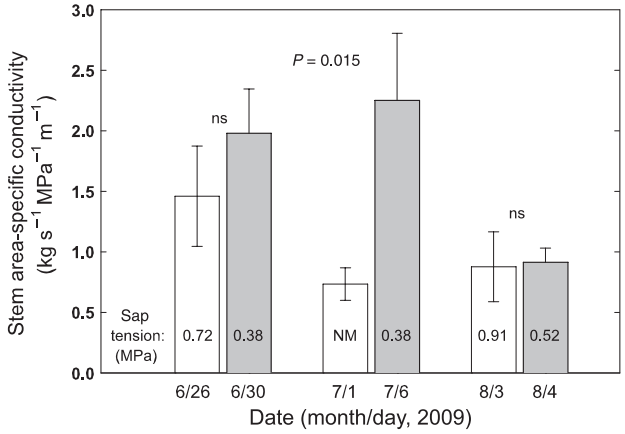

Fig. 2 Evidence of diurnal refilling in *Quercus gambelii* stems. Hydraulic conductivity per cross-sectional area at predawn (closed bars) and midday (open bars) for the indicated dates. Means ± SE; n = 5–10 stems per date; ns, not significant (P > 0.05). The average stem sap tension at the time of collection is indicated within each bar (NM, not measured).

1.5 MPa; Fig. 1, closed circles). Refilling was evident from repeatedly higher predawn relative to midday values (although not always significant), and appeared to cease later in the growing season when predawn sap tension failed to drop below 0.5 MPa (Fig. 2). Phloem girdling experiments early in the growing season substantially inhibited refilling (Fig. 3). One stem was inadvertently not completely girdled, and showed higher conductivity than the other fully girdled ones. This variation contributed to the marginal P value of 0.06. Nocturnal observations on a separate population of saplings, 3 km away, failed to discover positive sap pressure. Attempts to promote refilling later in the season by lowering xylem sap tension, either by shading treatments during

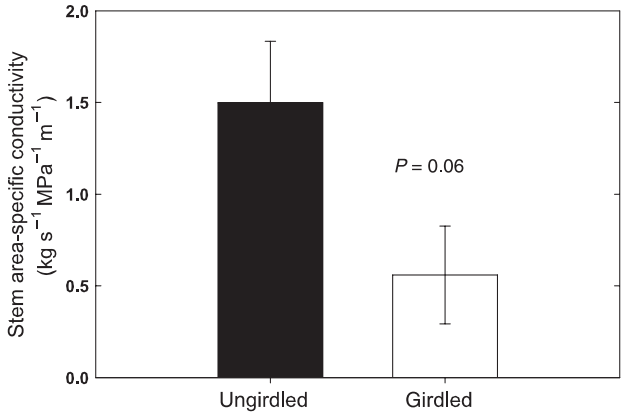

Fig. 3 Phloem girdling inhibits the recovery of stem hydraulic conductivity in *Quercus gambelii*. Stem conductivity per cross-sectional area at predawn for stems girdled the previous day (open bar) vs ungirdled controls (closed bar). Means ± SE, n = 5 per treatment.

the afternoon or sapling hydration experiments overnight, failed, possibly because sap tension was not substantially decreased by the treatments (mean tension of 0.71 MPa for the afternoon shading treatment and 0.68 MPa at predawn for the hydration treatment).

Dehydration vulnerability curve

Native conductivities, in combination with excised branch drydowns (Fig. 1, open squares), yielded a dehydration vulnerability curve. Drying branches above the native sap tension range continued the highly variable decline in conductivity. Some branches reached zero conductivity at or below 2 MPa, whereas others maintained limited conductivity to above 4 MPa. Overall, the dehydration curve showed a significant drop in conductivity between 0 and 1 MPa with a long tail of low conductivity reaching zero above 4 MPa. Fitting a Weibull function to the entire dataset (Fig. 1, solid curve, r^2 = 0.43) yielded a mean cavitation tension of 1.22 MPa (0.77, 1.62) and a median, or P50, of 1.08 MPa (0.44, 1.54).

Single-vessel air injections

Five hundred and three vessels were injected by the single-vessel method in eight 75-cm stems. Of this total, 44% were open vessels with no endwalls present, and 66% were closed off by at least one inter-vessel wall. Of the closed off vessel files, *c.* 40% had relatively low air-seeding pressures below 1.0 MPa (Fig. 4). However, the remaining 60% air-seeded over a wide range of evenly distributed pressures, with 11.5% exceeding 5 MPa (Fig. 4). The highest successful measurement was 6.6 MPa. In *c.* 10% of the injections, the capillary tube ruptured at high pressure (usually above 5 MPa) before air-seeding occurred. In no case did we risk raising the pressure above 7 MPa. These files (tube bursts or > 7 MPa) were scored as air-seeding above 6.6 MPa. There was no obvious difference in the air-seeding range of the eight tested stems: each stem had vessel files that air-seeded over the same broad range from below 0.2 MPa to above 4.5 MPa. The overall

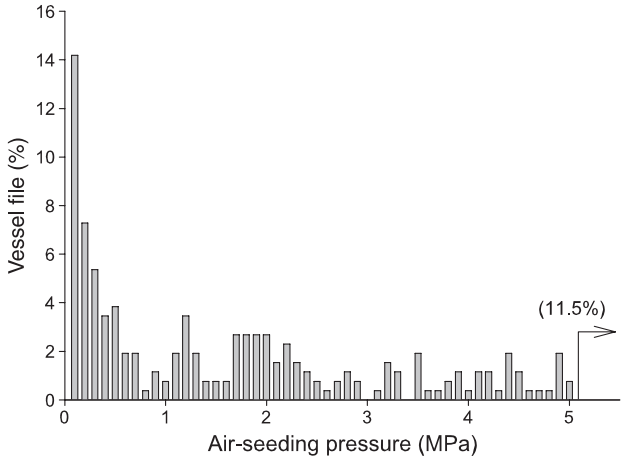

Fig. 4 Single-vessel air injections through 75-cm-long stems of *Quercus gambelii*. Percentage of vessel files (with one or more inter-vessel walls present) air-seeding at 0.1-MPa pressure increments. Open vessels (zero inter-vessel walls) are not included; 11.5% of injected vessels air-seeded above 5 MPa (arrow).

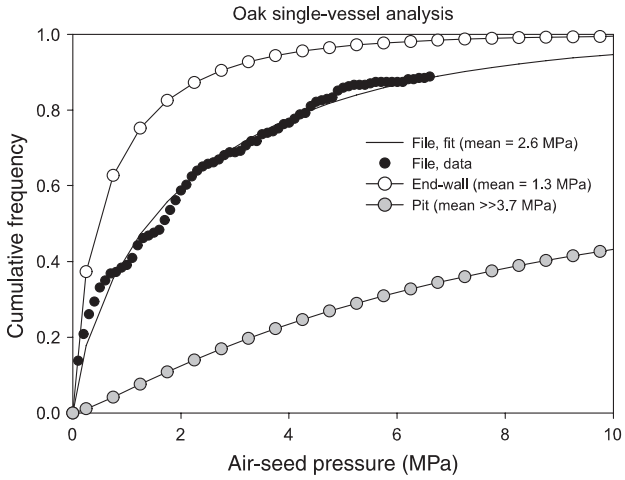

Fig. 5 Estimates of inter-vessel wall (endwall) and pit air-seeding pressures from single-vessel injection data in *Quercus gambelii*. Black circles show the cumulative distribution of the vessel file air-seeding pressure data from Fig. 4. The associated curve is the best-fit Weibull cumulative distribution function (CDF) for the file data (CDF_f). White circles show the estimated CDF for inter-vessel wall air-seeding (CDF_e, Eqn 1). Gray circles represent the estimated CDF for air-seeding through individual pits of inter-vessel walls (CDF_p, Eqn 2).

median failure pressure was 1.7 MPa (Fig. 5, CDF_f data), and the mean observed air-seeding pressure was 2.2 ± 0.12 MPa. Fitting a Weibull function to the observed cumulative distribution (Fig. 5, CDF_f line) extrapolated the missing high-pressure data (e.g. > 6.6 MPa) and yielded a lower estimated mean failure pressure of 2.58 MPa (2.52, 2.65). The injected vessels had a mean diameter of 122 ± 2 μm (n = 503), and the vessel diameter was not correlated with the air-seeding pressure (data not shown). There was a tendency for closely spaced vessels to air-seed at similar pressure.

The silicone injection and vessel length distribution analysis yielded a median vessel length of 0.73 m. This was roughly consistent with the above report of 44% of vessels being open in 0.75-m-long stems used for single-vessel injection. Of the remaining closed files, 37% were estimated to have one inter-vessel wall (= endwall), 27% had two endwalls and the remaining 36% of files had more than two endwalls in series (n_e, Eqn 1). The length distribution discretized into nine classes is shown in Table 1, together with the estimated number of pits (u_i, Eqn 2) and endwalls (e, n_e) for 75-cm stems. These parameters were used to solve Eqn 1 for the endwall failure CDF_e.

The file failure CDF_f in Eqn 1 was represented by the Weibull function fit to the single-vessel air injection data (Fig. 5, file CDF_f). Solving Eqn 1 yielded an endwall failure distribution (Fig. 5, endwall CDF_e). The file CDF_f was less leaky than the endwall CDF_e, reflecting the estimation that 63% of the closed files required the breaching of $e \geq 2$ endwalls in series. The average inter-vessel wall was estimated to air-seed at a pressure of 1.02 MPa (0.98, 1.06), a value similar to the mean cavitation tension from the dehydration curve (1.22 MPa (0.77, 1.62)).

The value of $1 - CDF_e(p)$ indicates the fraction of inter-vessel walls that withstand air-seeding up to pressure p. Assuming that conductivity declines in proportion to the breached inter-vessel walls, the $1 - CDF_e(p)$ value can be normalized by the maximum native conductivity (k) to yield a proxy for hydraulic conductivity at pressure p:

$$\text{conductivity}\ (p) = k \cdot [1 - CDF_e(p)] \qquad \text{Eqn 3}$$

Fitting Eqn 3 to the dehydration vulnerability curve (using k as a curve-fitting parameter) yielded a curve very similar to the dehydration vulnerability curve and with a similar r^2 value (Fig. 1, dash–dotted $1 - CDF_e$ line, r^2 = 0.42).

Solving Eqn 2 for the pit failure CDF_p yielded a very broad distribution of pit failure pressures (Fig. 5, gray pit CDF_p curve), with 7% failing below the mean air-seeding pressure of 1.22 MPa (the rare leaky pits) and 67% failing above 6.25 MPa (the majority of airtight pits). CDF_p beyond 6–7 MPa is not meaningful because it is unconstrained by data.

Discussion

The results supported the counter-intuitive, but predicted, presence of early-wood vessels that were extremely vulnerable to cavitation by air-seeding in the ring-porous *Q. gambelii.* The dehydration vulnerability curve showed a *c.* 50% drop in conductivity at sap tensions below 1 MPa, with a median cavitation tension (P50) of 1.08 MPa and a mean cavitation tension of 1.22 MPa (Fig. 1). The corollary expectation of a portion of cavitation-resistant vessels was also seen in the long tail on the dehydration curve, where conductivity was still present in some branches at tensions above 4 MPa. The distribution of vessel file air-seeding pressures mirrored the dehydration curve: a large fraction of early-wood vessel files exhibited very low air-seeding pressures, whereas a long tail extended maximum pressures beyond 5 MPa (Figs 4, 5). The estimated air-seeding of inter-

vessel walls (Fig. 5, CDF_e) closely matched the shape of the dehydration vulnerability curve (Fig. 1, dash–dotted vs solid curves). Inter-vessel walls were estimated to air-seed at an average of 1.02 MPa, similar to the mean cavitation tension of 1.22 MPa.

Simple probability theory (Eqns 1, 2) provided a baseline estimate of how rare the leaky pits need to be to explain the injection data. Only 7% of the inter-vessel pits were predicted to air-seed at the mean cavitation tension (1.22 MPa). The majority of pits were predicted to be airtight, with 67% expected to hold against sap tensions above 6.25 MPa, considerably more than enough to withstand the seasonal maximum of 1.5 MPa at the study site (Fig. 1). Deviations from theory assumption and analysis could change the exact predictions, but the major role of probability seems to be inescapable given the extremely wide range of observed air-seeding pressures in otherwise rather similar early-wood vessel files (Fig. 4). Injected vessel diameters clustered closely around an average of 122 ± 2 μm, and 66% of the closed files were expected to have just one to three endwalls in series (Table 1, n_e data). The stochasticity implied by the air injection data (Fig. 4) is also consistent with the considerable variation in native conductivities seen in the dehydration vulnerability curve (Fig. 1) and other experiments.

The same probability theory applied to whole-stem air-seeding pressures in *Acer* species also supported the rare presence of leaky pits, but predicted that they were even less frequent in *Acer* (Christman *et al.*, 2009). Only *c.* 0.01% of pits were expected to air-seed at the mean cavitation tension in three *Acer* species vs 7% in *Q. gambelii*. This could suggest a higher 'error rate' in the development of pits in *Q. gambelii*, something which could be investigated ultrastructurally. More prosaically, the difference could be an artifact of model structure, imperfect assumptions or input data collection. Encouragingly, our *Quercus* and earlier *Acer* studies are in general agreement in finding an approximate correspondence between the mean cavitation tension from vulnerability curves and the mean endwall air-seeding pressure of the CDF_e obtained from Eqn 1 (Fig. 1, solid vs dash–dotted curves). This suggests that any discrepancy between the *Acer* and *Quercus* studies is more likely to be in Eqn 2 for the pit CDF_p than in Eqn 1.

An important corollary result is that so-called '*r*'-shaped vulnerability curves are not necessarily artifactual. An '*r*'-shaped curve exhibits a steep drop in conductivity at low sap tensions before leveling off in a long tail (it is '*r*' shaped when plotted as PLC; the '*r*' shape is inverted in Fig. 1). Such curves generated by centrifugal or pressure-sleeve methods have been shown to disagree with sigmoidal dehydration curves in some species (Choat *et al.*, 2010; Cochard *et al.*, 2010). The dehydration protocol is generally considered to be the most artifact-free vulnerability curve method, because it allows sap tensions to be developed uniformly and naturally within the xylem. Yet, this trusted protocol yielded an '*r*'-shaped curve for *Q. gambelii* (Fig. 1, solid curve). Any tendency of bagged leaf tension to overestimate stem tension would only mean that the real curve is even more vulnerable than shown. Further validation of '*r*'-shaped curves comes from the '*r*'-shaped endwall air-seeding CDF_e (Fig. 1, dash–dotted curve; Fig. 5 endwall CDF_e), which is derived from the '*r*'-shaped file failure CDF_f that was measured directly using the single-vessel method (Fig. 5, file CDF_f data). In a related study (Sperry *et al.*, 2011), we found that a centrifuge vulnerability curve from the same *Q. gambelii* population was also '*r*' shaped and is similar to the dehydration curve shown here, despite the presence of 86% of vessels being open to the center of the spinning segment or beyond. Apparently, not all ring-porous species are equally prone to the open vessel artifact.

The evidence for vessel refilling confirms a previous report for *Q. gambelii* in the same watershed (Taneda & Sperry, 2008). For an embolized vessel to refill, the surrounding fluid pressure needs to rise at least close to atmospheric pressure, with above atmospheric pressures greatly increasing the refilling rate (Yang & Tyree, 1992). Positive pressures should result in the exudation of sap from cut vessels. Despite all-night vigils, we observed no evidence of sap exudation from any freshly cut vessels. These observations were not conclusive, however, because they had to be made on a separate population of saplings that may not have been refilling. Refilling was apparently quite sensitive to the bulk sap tension (i.e. tension of the nonembolized vessels), because it ceased when predawn tension rose above 0.5 MPa. The fact that refilling seemed to be occurring despite bulk xylem tensions in the 0.2–0.5-MPa range suggests that there is some kind of pumping mechanism to pressurize embolized vessels above the surrounding sap that is under tension. Such a pump would have to work harder against greater sap tension, perhaps explaining the 0.5-MPa threshold. *Laurus nobilis* was also observed to refill as long as tensions were < 0.6 MPa overnight (Salleo *et al.*, 2009). The pumping mechanism may be dependent on phloem transport, because it was inhibited by phloem girdling. Girdling also inhibited refilling in *L. nobilis* (Salleo *et al.* 2004, 2006, 2009), indicating that the role of phloem in refilling is likely to be widespread.

Given the seemingly indisputable evidence for a sizeable fraction of leaky and potentially vulnerable early-wood vessels in *Q. gambelii*, why have such leaky vessels evolved, and is the same true of all large-vesseled taxa? The rare pit hypothesis suggests that, at least in part, vulnerable vessels are the consequence of having larger vessels. Ring-porous trees rely on the conducting efficiency of large vessels to carry their water in a single growth ring. Even if many are also highly vulnerable to cavitation by water stress, those remaining obviously still carry enough water to supply the crown. The refilling capability seen in *Q. gambelii* can also partially compensate for cavitating vessels. It is also possible that leaky vessels are not all embolized *in vivo*, simply because they do not happen to be next to an air-filled vessel. This could explain discrepancies between magnetic resonance imaging (MRI) of embolism in intact vessel networks (Choat *et al.*, 2010) vs methods that expose the xylem to air and turn potential air-seeding sites into actual ones. Another potential problem with estimating water content by MRI is that it does not discriminate between immature vessels which are fluid-filled but not functioning in water transport vs functional mature vessels.

The vessel size–vulnerability tradeoff is likely to be quite complex, because circumventing mechanisms probably exist. Larger vessels do not necessarily require more pits depending on how

they are organized into a network (Hacke *et al.*, 2006). The degree of connectivity between vessels will also influence vulnerability to air-seeding (Loepfe *et al.*, 2007). Even if more pits are present in larger vessels, changes in pit quality (thicker membranes, for example) could offset any effect of increasing number on vulnerability to air-seeding (Choat *et al.*, 2008; Lens *et al.*, 2010). Therefore, it seems possible that not all large-vesseled species will be uniformly vulnerable. The observed variability in vulnerability vs vessel size relationships across species is no doubt the result of the mechanistic complexity of the tradeoff, as well as differences in selective pressures for efficiency vs safety across habitats and growth forms.

Acknowledgements

Financial support to J.S.S. was provided by NSF-IBN-0743148. The University of Utah Summer Undergraduate Research Program provided support for Taylor J. Workman who cheerfully assisted with field and laboratory work.

References

Bush SE, Pataki DE, Hultine KR, West AG, Sperry JS, Ehleringer JR. 2008. Wood anatomy constrains stomatal responses to atmospheric vapor pressure deficit in irrigated, urban trees. *Oecologia* **156**: 13–20.

Choat B, Ball M, Luly J, Holtum J. 2003. Pit membrane porosity and water stress-induced cavitation in four co-existing dry rainforest tree species. *Plant Physiology* **131**: 41–48.

Choat B, Cobb AR, Jansen S. 2008. Structure and function of bordered pits: new discoveries and impacts on whole-plant hydraulic function. *New Phytologist* **177**: 608–626.

Choat B, Drayton WM, Brodersen C, Matthews MA, Schackel KA, Wada H, McElrone AJ. 2010. Measurement of vulnerability to water stress-induced cavitation in grapevine: a comparison of four techniques applied to a long-vesseled species. *Plant, Cell & Environment* **33**: 1502–1512.

Christman MA, Sperry JS, Adler FR. 2009. Testing the rare pit hypothesis in three species of *Acer*. *New Phytologist* **182**: 664–674.

Cochard H, Gaelle D, Bodet C, Tharwat I, Poirier M, Ameglio T. 2005. Evaluation of a new centrifuge technique for rapid generation of xylem vulnerability curves. *Physiologia Plantarum* **124**: 410–418.

Cochard H, Herbette S, Barigah T, Vilagrosa A. 2010. Does sample length influence the shape of vulnerability to cavitation curves? A test with the Cavitron spinning technique *Plant, Cell & Environment* **33**: 1543–1552.

Cochard H, Tyree MT. 1990. Xylem dysfunction in *Quercus*: vessel sizes, tyloses, cavitation and seasonal changes in embolism. *Tree Physiology* **6**: 393–407.

Ennajeh M, Simoes F, Khemira H, Cochard H. 2011. How reliable is the double-ended pressure sleeve technique for assessing xylem vulnerability to cavitation in woody angiosperms? *Physiologia Plantarum* **142**: 205–210.

Hacke UG, Sperry JS, Wheeler JK, Castro L. 2006. Scaling of angiosperm xylem structure with safety and efficiency. *Tree Physiology* **26**: 689–701.

Hargrave KR, Kolb KJ, Ewers FW, Davis SD. 1994. Conduit diameter and drought-induced embolism in *Salvia mellifera* Greene (Labiatae). *New Phytologist* **126**: 695–705.

Lens F, Sperry JS, Christman MA, Choat B, Rabaey D, Jansen S. 2010. Testing hypotheses that link wood anatomy to cavitation resistance and hydraulic conductivity in the genus *Acer*. *New Phytologist* **190**: 709–723.

Li Y, Sperry JS, Taneda H, Bush SE, Hacke UG. 2008. Evaluation of centrifugal methods for measuring xylem cavitation in conifers, diffuse- and ring-porous angiosperms. *New Phytologist* **177**: 558–568.

Loepfe L, Martinez-Vilalta J, Pinol J, Mencuccini M. 2007. The relevance of xylem network structure for plant hydraulic efficiency and safety. *Journal of Theoretical Biology* **247**: 788–803.

Pockman WT, Sperry JS. 2000. Vulnerability to cavitation and the distribution of Sonoran desert vegetation. *American Journal of Botany* **87**: 1287–1299.

Salleo S, LoGullo MA, Trifilo P, Nardini A. 2004. New evidence for a role of vessel-associated cells and phloem in the rapid xylem refilling of cavitated stems of *Laurus nobliis* L. *Plant, Cell & Environment* **27**: 1065–1076.

Salleo S, Trifilo P, Esposito S, Nardini A, LoGullo MA. 2009. Starch-to-sugar conversion in wood parenchyma of field growing *Laurus nobilis* plants: a component of the signal pathway for embolism repair? *Functional Plant Biology* **36**: 815–825.

Salleo S, Trifilo P, LoGullo MA. 2006. Phloem as a possible major determinant of rapid cavitation reversal in stems of *Laurus nobilis* (laurel). *Functional Plant Biology* **31**: 1063–1074.

Sperry JS, Christman MA, Torres-Ruiz JM, Taneda H, Smith DD. 2011. Vulnerability curves by centrifugation: is there an open vessel artifact, and are 'r' shaped curves necessarily invalid? *Plant, Cell & Environment*. doi: 10.1111/j.1365-3040.2011.02439.x

Sperry JS, Tyree MT. 1988. Mechanism of water stress-induced xylem embolism. *Plant Physiology* **88**: 581–587.

Sperry JS, Donnelly JR, Tyree MT. 1988. A method for measuring hydraulic conductivity and embolism in xylem. *Plant, Cell & Environment* **11**: 35–40.

Taneda H, Sperry JS. 2008. A case-study of water transport in co-occurring ring-versus diffuse-porous trees: contrasts in water-status, conducting capacity, cavitation and vessel refilling. *Tree Physiology* **28**: 1641–1652.

Tyree MT, Davis SD, Cochard H. 1994. Biophysical perspectives of xylem evolution - is there a tradeoff of hydraulic efficiency for vulnerability to dysfunction? *International Association of Wood Anatomists Journal* **15**: 335–360.

Tyree MT, Sperry JS. 1989. Vulnerability of xylem to cavitation and embolism. *Annual Review of Plant Physiology* **40**: 19–38.

Wang J, Ives N, Lechowicz M. 1992. The relation of foliar phenology to xylem embolism in trees. *Functional Ecology* **6**: 469–475.

Wheeler JK, Sperry JS, Hacke UG, Hoang N. 2005. Inter-vessel pitting and cavitation in woody Rosaceae and other vesselled plants: a basis for a safety vs. efficiency trade-off in xylem transport. *Plant, Cell & Environment* **28**: 800–812.

Yang S, Tyree MT. 1992. A theoretical model of hydraulic conductivity recovery from embolism with comparison to experimental data on *Acer saccharum*. *Plant, Cell & Environment* **15**: 633–643.

Zimmermann MH. 1983. *Xylem structure and the ascent of sap: Springer Series in Wood Science*. Berlin, Germany, Heidelberg, Germany, New York, USA: Springer.

Zimmermann MH, Brown CL. 1971. *Trees: structure and function*. Berlin, Germany: Springer-Verlag.

Zwieniecki MA, Melcher PJ, Holbrook NM. 2001. Hydraulic properties of individual xylem vessels of *Fraxinus americana*. *Journal of Experimental Botany* **52**: 257–264.